



Kinetics of stabilised Criegee intermediates derived from alkene ozonolysis: reactions with SO₂, H₂O and decomposition under boundary layer conditions

Journal:	<i>Physical Chemistry Chemical Physics</i>
Manuscript ID:	CP-ART-09-2014-004186.R1
Article Type:	Paper
Date Submitted by the Author:	19-Dec-2014
Complete List of Authors:	Newland, Mike; University of Birmingham, School of Geography, Earth and Environmental Sciences Rickard, Andrew; National Centre for Atmospheric Science (NCAS), University of York, Alam, Mohammed; University of Birmingham, School of Geography, Earth and Environmental Sciences Vereecken, Luc; Max Planck Institute for Chemistry, Atmospheric Sciences Muñoz, Amalia; Instituto Universitario CEAM-UMH, EUPHORE Laboratories Ródenas, Milagros; Instituto Universitario CEAM-UMH, EUPHORE Laboratories Bloss, William; University of Birmingham, School of Geography, Earth and Environmental Sciences

Kinetics of stabilised Criegee intermediates derived from alkene ozonolysis: reactions with SO₂, H₂O and decomposition under boundary layer conditions

Cite this: DOI: 10.1039/x0xx00000x

Mike J. Newland^a, Andrew R. Rickard^b, Mohammed S. Alam^a, Luc Vereecken^c, Amalia Muñoz^d, Milagros Ródenas^d, William J. Bloss^a,

Received 00th January 2012,
Accepted 00th January 2012

DOI: 10.1039/x0xx00000x

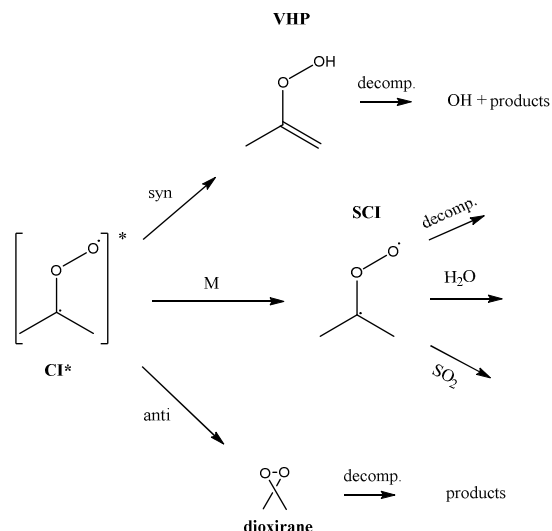
www.rsc.org/

The removal of SO₂ in the presence of alkene-ozone systems has been studied for ethene, *cis*-but-2-ene, *trans*-but-2-ene and 2,3-dimethyl-but-2-ene, as a function of humidity, under atmospheric boundary layer conditions. The SO₂ removal displays a clear dependence on relative humidity for all four alkene-ozone systems confirming a significant reaction for stabilised Criegee intermediates (SCI) with H₂O. The observed SO₂ removal kinetics are consistent with relative rate constants, $k(\text{SCI} + \text{H}_2\text{O}) / k(\text{SCI} + \text{SO}_2)$, of $3.3 (\pm 1.1) \times 10^{-5}$ for CH₂OO, $26 (\pm 10) \times 10^{-5}$ for CH₃CHOO derived from *cis*-but-2-ene, $33 (\pm 10) \times 10^{-5}$ for CH₃CHOO derived from *trans*-but-2-ene, and $8.7 (\pm 2.5) \times 10^{-5}$ for (CH₃)₂COO derived from 2,3-dimethyl-but-2-ene. The relative rate constants for $k(\text{SCI decomposition}) / k(\text{SCI} + \text{SO}_2)$ are $-2.3 (\pm 3.5) \times 10^{11} \text{ cm}^3$ for CH₂OO, $13 (\pm 43) \times 10^{11} \text{ cm}^3$ for CH₃CHOO derived from *cis*-but-2-ene, $-14 (\pm 31) \times 10^{11} \text{ cm}^3$ for CH₃CHOO derived from *trans*-but-2-ene and $63 (\pm 14) \times 10^{11} \text{ cm}^3$ for (CH₃)₂COO. Uncertainties are $\pm 2\sigma$ and represent combined systematic and precision components. These values are derived following the approximation that a single SCI is present for each system; a more comprehensive interpretation, explicitly considering the differing reactivity for *syn*- and *anti*- SCI conformers, is also presented. This yields values of $3.5 (\pm 3.1) \times 10^{-4}$ for $k(\text{SCI} + \text{H}_2\text{O}) / k(\text{SCI} + \text{SO}_2)$ of *anti*-CH₃CHOO and $1.2 (\pm 1.1) \times 10^{13}$ for $k(\text{SCI decomposition}) / k(\text{SCI} + \text{SO}_2)$ of *syn*-CH₃CHOO. The reaction of the water dimer with CH₂OO is also considered, with a derived value for $k(\text{CH}_2\text{OO} + (\text{H}_2\text{O})_2) / k(\text{CH}_2\text{OO} + \text{SO}_2)$ of $1.4 (\pm 1.8) \times 10^{-2}$. The observed SO₂ removal rate constants, which technically represent upper limits, are consistent with decomposition being a significant, structure dependent, sink in the atmosphere for *syn*-SCI.

1. Introduction

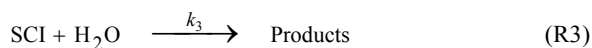
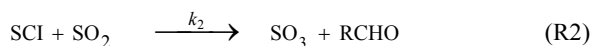
Atmospheric oxidation processes are central to understanding trace gas atmospheric composition, the abundance of air pollutants harmful to human health, crops and ecosystems, and the removal of reactive greenhouse gases such as methane. The principal atmospheric oxidants responsible for initiating the gas-phase degradation of volatile organic compounds (VOCs), NO_x and SO₂ are OH, NO₃ and O₃, with additional contributions from other species such as halogen atoms. Recent field measurements¹ in a boreal forest have identified the presence of an additional oxidant species, removing SO₂ and producing H₂SO₄. The additional SO₂ oxidation observed was substantial (comparable to that due to OH radicals alone), and attributed to a product of alkene ozonolysis – the boreal forest environment being one in which substantial biogenic alkene emissions occur – suggested to be the stabilised Criegee intermediate (SCI). The gas-phase oxidation of SO₂ in the atmosphere is of interest to climate research as it leads to formation of H₂SO₄, contributing to new particle formation and sulphate aerosol loading, in competition with condensed phase oxidation². A missing mechanism for the

conversion of SO₂ to H₂SO₄ could lead to model underestimation of the sulphate aerosol burden and affect radiative forcing calculations³, with corresponding implications for climate predictions. Enhanced SO₂ oxidation in alkene-ozone systems was first reported by Cox & Penkett⁴ over forty years ago, however the precise reaction mechanism giving rise to this effect remains elusive. The ‘‘Criegee’’ ozonolysis reaction mechanism was first postulated in the 1940s⁵. It is now accepted that the ozone molecule adds to the C=C double bond via a concerted cycloaddition to form a primary ozonide, followed by cleavage of the C-C bond and one of the O-O bonds forming a carbonyl molecule and a carbonyl oxide, or ‘Criegee intermediate’ (CI)⁶. Ozonolysis derived SCIs are formed with a broad internal energy distribution, to yield chemically activated and stabilised SCIs. SCIs can have sufficiently long lifetimes to undergo bimolecular reactions with H₂O and SO₂ amongst other species. Chemically activated SCIs may also undergo collisional stabilisation, unimolecular decomposition or isomerisation (Scheme 1). For substituted alkenes, SCIs can undergo a 1,4 H-shift rearrangement through a



Scheme 1 Simplified mechanism for the reaction of Criegee Intermediates (CIs) formed from alkene ozonolysis.

vinyl-hydroperoxide (VHP) via the so-called “hydroperoxide channel” and decompose to yield OH and a vinyloxy radical – a substantial non-photolytic source of atmospheric oxidants^{7,8}. This is the favoured channel for SCIs formed in the *syn*-configuration. Time resolved studies⁹ show that the VHP may persist for appreciable timescales under boundary layer conditions, giving rise to the observed pressure dependence of OH radical yields¹⁰, and opening the possibility for bimolecular reactions of this species to occur. SCIs formed in the *anti*-configuration are thought to primarily undergo rearrangement and decomposition via a dioxirane intermediate (“the acid/ester channel”), producing a range of daughter products and contributing to the observed overall HO_x radical yield^{6,11}.



Until recently, it has been thought that the predominant atmospheric fate for SCIs was reaction with water vapour^{12,13} – leading to a significant source of organic acids and hydroperoxides, suggesting that bimolecular reaction with SCIs is an unimportant oxidation mechanism for trace gas species. This view was recently challenged by direct observation¹⁴ and kinetic studies^{15,16,17} of the CH₂OO and CH₃CHOO SCIs.

Taatjes and co-workers¹⁵, directly observing CI kinetics for the first time, found reactions of CH₂OO with SO₂ and NO₂ to be substantially faster than previously thought, pointing to a potentially important role for this species in atmospheric SO₂ and NO₂ oxidation; subsequent measurements have identified SO₃¹⁶ and NO₃¹⁸ as products of these reactions. The key to whether SCIs are indeed significant contributors to gas-phase atmospheric SO₂ oxidation is the ratio of the rate constants for reaction of the SCI with SO₂ (k_2), to that with H₂O (k_3) and decomposition (k_d). In laboratory studies where SCIs were produced by the 248 nm laser photolysis of alkyl iodide precursors at 4 Torr total pressure, with the SCI decay monitored by VUV photoionisation in the presence of

excess co-reactants, this ratio has recently been reported to be 10³ – 10⁴ for the smallest two SCIs (CH₂OO^{15,17} and CH₃CHOO¹⁶), with k_2 on the order of 10⁻¹¹ cm³ s⁻¹ and k_3 on the order of 10⁻¹⁵ cm³ s⁻¹. In contrast, alternative studies of SO₂ oxidation in alkene-ozone systems, performed at atmospheric pressure through detection of the H₂SO₄ product, find much smaller SCI + SO₂ rate coefficients (by *ca.* two orders of magnitude)¹⁹. Explanations for this apparent discrepancy may include the lifetime of the secondary ozonide (SOZ) adduct formed from the SCI + SO₂ reaction, collisionally stabilised at atmospheric pressure²⁰, effects of the presence of multiple SCI conformers with differing reactivity, or contributions from other oxidant species, formed within the ozonolysis system, to SO₂ reaction. Understanding the behaviour of the ozone-alkene-SO₂ system in the presence of water vapour is critical to quantifying the impact of SCI chemistry upon atmospheric SO₂ oxidation²¹.

An additional, potentially important, fate of SCI under atmospheric conditions is unimolecular decomposition (denoted k_d in (R4)). For CH₂OO, rearrangement via a ‘hot’ acid species represents the lowest accessible decomposition channel, but due to lack of alkyl substituents, the theoretically predicted 298 K rate constant is rather low, 0.3 s⁻¹²². Previous studies have identified the hydroperoxide rearrangement as dominant for SCIs with a *syn* configuration, determining their overall unimolecular decomposition rate^{7,8}. For *syn*-CH₃CHOO recent experimental²³ work yielded a decomposition rate of 3 – 30 s⁻¹. Theoretical work²⁴ has predicted a decomposition rate coefficient of 24.2 s⁻¹ for *syn*-CH₃CHOO and 67.2 s⁻¹ for *anti*-CH₃CHOO (for which only the ester channel exists), owing to the potential energy release from the higher energy *anti*-conformer²³. An upper limit to total CH₃CHOO loss (decomposition and heterogeneous wall losses combined) of < 250 s⁻¹ has been reported by Taatjes *et al.*¹⁶ Earlier experimental work reported decomposition rate constants of ≤ 20 s⁻¹ for CH₃CHOO derived from *cis*-but-2-ene ozonolysis²⁵, and 76 s⁻¹ (accurate to within a factor of three) for CH₃CHOO derived from *trans*-but-2-ene ozonolysis²⁶. For (CH₃)₂COO (derived from 2,3-dimethyl-but-2-ene ozonolysis) a total loss rate of 3.0 s⁻¹ has recently been determined experimentally¹⁹. This value (which represents an upper limit for k_d) is somewhat smaller than but comparable in magnitude to an earlier measurement of 6.4 s⁻¹ (determined at 100 Torr)²⁷. Theoretical estimates of (CH₃)₂COO decomposition rates are higher, at up to 250 s⁻¹²². Photolysis loss rates have also recently been reported for CH₂OO²⁸ and CH₃CHOO²⁹ of 1 s⁻¹ and 0.2 s⁻¹ respectively, calculated for actinic flux values at midday, SZA = 0°.

Here, we present results of a series of experiments in which the oxidation of SO₂ during the ozonolysis of ethene, *cis*-but-2-ene, *trans*-but-2-ene and 2,3-dimethyl-but-2-ene (tetramethylethylene, TME), was investigated in the presence of varying amounts of water in the European Photochemical Reactor facility (EUPHORE), Valencia, Spain.

2. Experimental

2.1 EUPHORE

EUPHORE is a 200 m³ simulation chamber used for studying reaction mechanisms under atmospheric boundary layer conditions. In general, experiments comprised time-resolved measurement of the removal of SO₂ in the presence of an alkene-ozone system, as a function of humidity. SO₂ and O₃ abundance were measured using conventional fluorescence and UV absorption monitors, respectively; alkene abundance was determined via FTIR spectroscopy. The precision of the SO₂ and O₃ monitors were 0.25 and 0.47 ppbv respectively (evaluated as 2 standard deviations of the

measured value prior to SO₂ or O₃ addition). The chamber is fitted with large horizontal and vertical fans to ensure rapid mixing (three minutes). Further details of the chamber setup and instrumentation are available elsewhere^{30,31}. Experiments were performed in the dark (*i.e.* with the chamber housing closed; $j(\text{NO}_2) \leq 10^{-6} \text{ s}^{-1}$), at atmospheric pressure (*ca.* 1000 mbar) and temperatures between 296 and 303 K, on timescales of *ca.* 20 – 30 minutes. Chamber dilution was monitored via the first order decay of an aliquot of SF₆, added prior to each experiment. Cyclohexane (*ca.* 75 ppmv) was added at the beginning of each experiment to act as an OH scavenger, such that SO₂ reaction with OH was calculated to be $\leq 1\%$ of the total chemical SO₂ removal in all experiments.

2.2 Experimental Approach

Experimental procedure, starting with the chamber filled with clean air, comprised addition of SF₆ and cyclohexane, followed by water vapour, O₃ (*ca.* 500 ppbv) and SO₂ (*ca.* 50 ppbv). A gap of five minutes was left prior to addition of the alkene, to allow complete mixing. The reaction was then initiated by addition of the alkene (*ca.* 500 ppbv for ethene, 200 ppbv for *cis*- and *trans*-but-2-ene and 400 ppbv for TME). The chamber was monitored for an hour subsequent to the addition of ethene and forty five minutes for *cis*- and *trans*-but-2-ene and TME. The rate of alkene/ozone consumption is dependent on k_f . Roughly 25% of the ethene was consumed after an hour, while for *cis*- and *trans*-but-2-ene and TME 90% of the alkene was consumed within roughly 25 minutes, 20 minutes and 6 minutes respectively. Each experiment was performed at a constant humidity, which was increased in a step-wise manner for consecutive runs to cover the range 1.5 – 21 % RH. Measured increases in [SO₂] agreed with measured volumetric addition across the SO₂ and humidity range used in the experiments.

2.3 Analysis Approach

The following sections describe (i) a common analysis applied to all systems, but which features several approximations, and (ii) more detailed consideration of each chemical system in turn, to address potential contributions from the water dimer, and multiple contributions within each system (*e.g.* contrasting reactivity of different SCI conformers).

From the chemistry presented in Reactions R1 – R4 it is assumed that SCI will be produced in the chamber from the reaction of the alkene with ozone at a given yield, ϕ . The SCI produced can then react with SO₂, with H₂O, with other species or decompose under the experimental conditions applied. The rate at which SO₂ is lost, compared with the total production of SCI, is determined by the fraction, f , of the total SCI produced which reacts with SO₂, compared to the sum of the total loss processes of the SCI (Equation E1):

$$f = \frac{k_2[\text{SO}_2]}{k_2[\text{SO}_2] + k_3[\text{H}_2\text{O}] + k_d + L} \quad (\text{E1})$$

$$\frac{d\text{SO}_2}{d\text{O}_3} = \phi \cdot f \quad (\text{E2})$$

Here, L is the sum of any other pseudo-first order chemical loss processes for SCI in the chamber, after correction for dilution, and neglecting other (non-alkene) chemical sinks for O₃, such as reaction

with HO₂ - also produced directly during alkene ozonolysis¹¹, but indicated through model calculations to account for $< 2\%$ of ozone loss under all the experimental conditions of this work. Equations E1 and E2 treat the SCIs formed as a single species – this is the case for (*e.g.*) ethene and TME, but is an approximation for the 2-butenes; considered further below.

2.3.1 SCI yield calculation

Values for ϕ_{SCI} were determined for each ozonolysis reaction from experiments performed under dry conditions (RH $< 1\%$) in the presence of excess SO₂ (*ca.* 1000 ppbv), such that SO₂ scavenges the overwhelming majority of the SCI. From Equation E2, regressing $d\text{SO}_2$ against $d\text{O}_3$ (corrected for chamber dilution), assuming f to be unity (*i.e.* all the SCI produced reacts with SO₂) determines the value of ϕ_{min} , a lower limit to the SCI yield. Figure 2 shows the experimental data, from which ϕ_{min} was derived, for all four alkene ozonolysis systems studied.

The lower limit criterion applies as in reality f will be less than one, at experimentally accessible SO₂ levels, as a small fraction of the SCI will still react with any H₂O present, or undergo decomposition. The actual yield, ϕ , was determined by combining the results from the high-SO₂ experiments with those from the series of experiments performed at lower SO₂, as a function of [H₂O], to determine k_3/k_2 and k_d/k_2 (see Section 2.3.2), through an iterative process to determine the single unique value of ϕ_{SCI} which fits both datasets. It is important to note that the SCI yield is to an extent an operationally defined quantity – for example, OH formation from alkene ozonolysis is known to proceed over at least hundreds of milliseconds⁹ following the alkene-ozone reaction, and so the corresponding CI population must also be evolving with time. In this work, SCI yields reflect the amount of SCI available to oxidise SO₂ on timescales of seconds to minutes.

2.3.2 $k(\text{SCI}+\text{H}_2\text{O})/k(\text{SCI}+\text{SO}_2)$ and $k_d/k(\text{SCI}+\text{SO}_2)$

To determine k_3/k_2 and k_d/k_2 , a series of experiments were performed for each alkene, in which the SO₂ loss was monitored as a function of [H₂O]. From Equation E2, regression of the loss of ozone ($d\text{O}_3$) against the loss of SO₂ ($d\text{SO}_2$) (both corrected for dilution, measured through the removal SF₆, added at the start of each experiment and monitored via FTIR) for an experiment determines the factor $f \phi$ at a given point in time. This quantity will vary through the experiment as SO₂ is consumed, and other potential SCI co-reactants are produced, as predicted by Equation E1. A smoothed fit was applied to the experimental data for the cumulative consumption of SO₂ and O₃, ΔSO_2 and ΔO_3 , (Figure 1) to determine $d\text{SO}_2/d\text{O}_3$ (and hence $f \phi$) at the start of each experiment, for use in Equation E3. The start of the experiment (*i.e.* when [SO₂] \sim 50 ppbv) was used as this corresponds to the greatest rate of production of the SCI, and hence largest experimental signals (O₃ and SO₂ rate of change) and is the point at which the SCI + SO₂ reaction has the greatest magnitude compared with any other potential chemical loss processes for either species (see discussion below).

$$[\text{SO}_2] \left(\frac{1}{f} - 1 \right) = \frac{k_3}{k_2} [\text{H}_2\text{O}] + \frac{k_d + L}{k_2} \quad (\text{E3})$$

The value $[\text{SO}_2]((1/f) - 1)$ can then be regressed against [H₂O] for each experiment to give a plot with a gradient of k_3/k_2 and an intercept of $(k_d + L)/k_2$ (Equation E3). Our data cannot determine

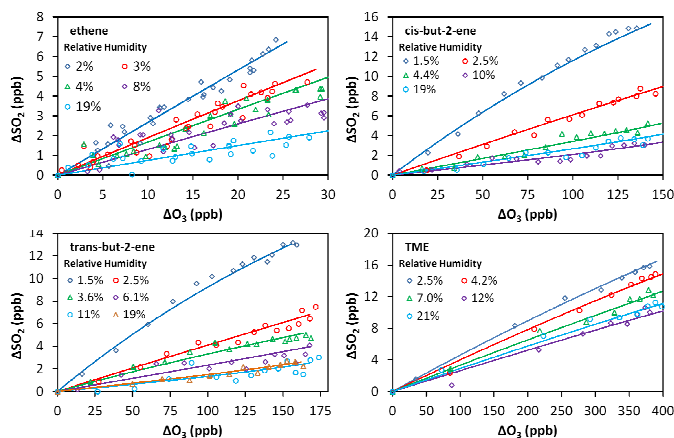


Figure 1 Cumulative consumption of SO_2 and O_3 , ΔSO_2 versus ΔO_3 , for the ozonolysis of four alkenes in the presence of SO_2 at a range of relative humidities from 1.5 – 21%. Open symbols are experimental data, corrected for chamber dilution. Solid lines are smoothed fits to the experimental data.

absolute rate constants (*i.e.* values of k_2 , k_3 , k_d) in isolation, but is limited to assessing their relative values, which may be placed on an absolute basis through use of an (external) reference value. Equations E1 – E3 as presented above assume that only a single SCI species is present in each ozonolysis system. While this is the case for the ethene and TME systems, for the but-2-ene systems this is an approximation as two conformers of the CH_3CHOO SCI (*syn* and *anti*) are produced. Further analysis is performed in Section 3.3.2 in which the SO_2 loss in the but-2-ene systems is treated as having two components, related to the different SCI.

3. Results and Discussion

3.1 Introduction

Table 1 shows the resulting SCI yields obtained for the ozonolysis of ethene, *cis*-but-2-ene, *trans*-but-2-ene and tetramethylethylene (TME); uncertainties are $\pm 2\sigma$, and represent the combined systematic (estimated measurement uncertainty) and precision components. Also shown are past literature values, obtained under various conditions using a range of different SCI scavengers.

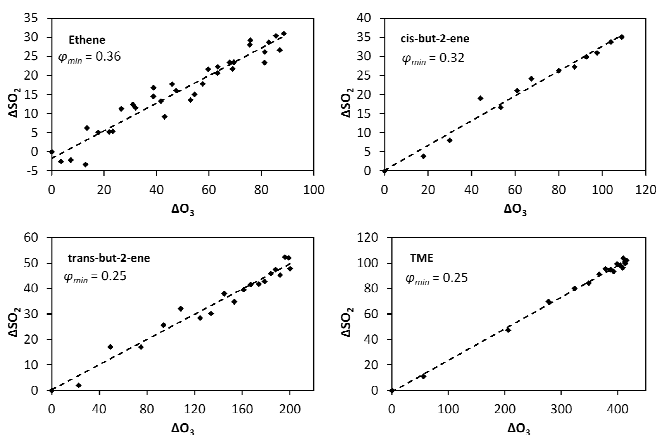


Figure 2 ΔSO_2 .v. ΔO_3 during the excess SO_2 experiments, to determine the minimum SCI yield for the four alkenes.

Table 1 SCI yields derived in this work and reported in the literature. Uncertainty ranges ($\pm 2\sigma$, parentheses) indicate combined precision and systematic measurement error components for this work, and are given as stated for literature studies. All referenced studies were conducted between 700 and 760 Torr. C2B – derived from *cis*-but-2-ene; T2B – derived from *trans*-but-2-ene.

SCI	ϕ_{SCI}	Reference
CH_2OO	0.37 (± 0.04)	This work
	0.37	MCMv3.2 ^a (IUPAC) ³³
	0.35 (± 0.05)	Niki <i>et al.</i> ³⁴
	0.39 (± 0.053)	Hatakeyama <i>et al.</i> ³⁵
	0.47 (± 0.05)	Horie and Moortgat ³⁶
	0.50 (± 0.04)	Neeb <i>et al.</i> ³⁷
	0.39 (± 0.11)	Hasson <i>et al.</i> ³⁸
0.54 (± 0.15)	Alam <i>et al.</i> ³¹	
CH_3CHOO (C2B)	0.38 (± 0.05)	This work
	0.19	Rickard <i>et al.</i> ³⁹
	0.18	Niki <i>et al.</i> ⁴⁰
	0.43	Cox and Penkett ⁴¹
	0.45	Cox and Penkett ⁴¹
CH_3CHOO (T2B)	0.28 (± 0.03)	This work
	0.49 (± 0.22)	Berndt <i>et al.</i> ³²
	0.53 (± 0.24)	Berndt <i>et al.</i> ¹⁹
	0.45	Cox and Penkett ⁴¹
	0.19 (± 0.03)	Hatakeyama <i>et al.</i> ³⁵
	0.42	Horie and Moortgat ³⁶
	0.24 (± 0.07)	Hasson <i>et al.</i> ³⁸
0.13	Rickard <i>et al.</i> ³⁹	
$(\text{CH}_3)_2\text{COO}$	0.32 (± 0.02)	This work
	0.45 (± 0.20)	Berndt <i>et al.</i> ³²
	0.62 (± 0.28)	Berndt <i>et al.</i> ¹⁹
	<i>ca.</i> 0.65 ^b	Drozd <i>et al.</i> ¹⁰
	0.10 (± 0.03)	Hasson <i>et al.</i> ³⁸
	0.30	Niki <i>et al.</i> ⁴⁰
	0.11	Rickard <i>et al.</i> ³⁹

^a <http://mcm.leeds.ac.uk/MCM/>

^b At 700–760 Torr (low pressure limit of 0.15 at 0 Torr).

The yield of CH_2OO from ethene ozonolysis obtained in this work is 0.37 (± 0.04). This yield has been investigated in many previous studies, with values ranging from 0.34 – 0.50 determined – a more detailed review is available elsewhere³¹. The yield obtained in this work is at the lower end of this range but within the envelope of these estimates, and is in excellent agreement with the current IUPAC recommendation of 0.37.

The yield of CH_3CHOO from *cis*-but-2-ene ozonolysis obtained in this work is 0.38 (± 0.05), with that from *trans*-but-2-ene being 0.28 (± 0.03). These values fall within the range of reported literature values of 0.18 – 0.43 and 0.13 – 0.53 for *cis*-but-2-ene and *trans*-but-2-ene respectively (Table 1). *Cis* and *trans*-but-2-ene both yield (differing) mixtures of *syn* and *anti* conformers of CH_3CHOO , the relative amounts of which are not well known, and which are treated here initially as a single SCI species (this approximation is discussed further in Section 3.3). Berndt *et al.*³² recently reported a yield of 0.49 (± 0.22) for the CH_3CHOO produced from *trans*-but-2-ene ozonolysis (also treating both *syn* and *anti* conformers as a single SCI species).

The yield of $(\text{CH}_3)_2\text{COO}$ from TME ozonolysis obtained in this work is 0.32 (± 0.02). This again falls within the (wide) range in the literature of 0.10 – 0.65, with Berndt *et al.*³² most recently reporting a yield of 0.45 (± 0.20).

Figure 1 shows the cumulative consumption of SO_2 relative to that of O_3 , ΔSO_2 versus ΔO_3 (after correction for dilution), as a function of $[\text{H}_2\text{O}]$ for each experiment for the four alkenes studied. A fit to each experiment, extrapolating the experimental data to evaluate $d\text{SO}_2/d\text{O}_3$ at $t = 0$ (start of each experimental run) for use in

Equations E1 – E3, is also shown. The overall change in SO_2 , ΔSO_2 , is seen to decrease substantially with increasing humidity (over a relatively narrow range of RH (1.5–20 %)) for all four alkenes. This trend would be expected from the understood chemistry (R1 – R4), as there is competition between SO_2 , H_2O , and decomposition for reaction with the SCI.

Figure 3 shows a fit of Equation E3 to the data for each alkene, giving a slope of k_3/k_2 and an intercept of $(k_d + L)/k_2$. The results appear to show a generally linear relationship; however, for *cis*- and *trans*-but-2-ene and TME, the data point at the highest relative humidity accessible in this work ($[\text{H}_2\text{O}] = 1.5\text{--}2.0 \times 10^{17} \text{ cm}^{-3}$) appears to deviate from this relationship. These data points lie outside the 95 % confidence intervals defined by all the other (lower relative humidity) data for each alkene. For the analysis to determine k_3/k_2 and $(k_d + L)/k_2$ presented in presented in Table 2, the points at the highest RH are excluded and the kinetic parameters are derived from a linear fit to the measurements from all other experiments. Extended analyses to account for the non-linearity observed for CH_3CHOO and $(\text{CH}_3)_2\text{COO}$ are presented in the following sections.

One potential explanation for the observed curvature in the CH_3CHOO and $(\text{CH}_3)_2\text{COO}$ data is measurement error. ΔSO_2 is relatively small at high $[\text{H}_2\text{O}]$ compared to the precision of the measurements; however, even allowing for associated uncertainties, the points at high RH do not fit the linear relationship successfully applied to the remaining data points. Moreover, any systematic error in the measurement of O_3 , SO_2 or H_2O would also be expected to affect the results for the ethene system (and to a greater extent, given the slow ethene-ozone reaction rate and consequent lower overall chemical SO_2 loss observed), suggesting that the cause lies in contrasting chemical behaviour. In terms of experimental factors, H_2O was measured using multiple approaches (two dew-point hygrometers in addition to a solid state probe) with no evidence for any divergence with RH. SO_2 monitors can exhibit humidity-dependent interferences (quenching of the SO_2 signal), commonly of the order of a few percent, observed at very high RH, and corrected through incorporation of a nafion dryer (fitted in this case); in addition the monitor-derived SO_2 concentration increments were in agreement with those calculated from the measured SO_2 addition and chamber volume, across the relative humidity range studied.

It should be noted that the k_d values reported here represent upper limits, as a consequence of possible further chemical losses for the SCI within our experimental system (as represented by L in Equation E3, notwithstanding the approach of extrapolating to the start of each experiment to minimise these). Other potential fates for SCIs include reaction with ozone^{42,43}, other SCI⁴³, carbonyl products⁴⁴, acids⁴⁵, or with the parent alkene⁴³ itself. Sensitivity analyses indicate that the reaction with ozone could be significant, as predicted by theory^{42,43} with a possible contribution of up to 10 % of SCI loss for $(\text{CH}_3)_2\text{COO}$ at 2 % RH, while total losses from reaction with SCI (self-reaction), carbonyls and alkenes are calculated to account for < 1 % of the total SCI loss under the experimental conditions applied.

3.2 CH_2OO

3.2.1 Linear Fit

For CH_2OO a linear fit (*i.e.* using Equation E3 vs. H_2O) describes the observations well (Figure 3) over the entire $[\text{H}_2\text{O}]$ range studied ($1\text{--}20 \times 10^{16}$ molecules cm^{-3}). This fit gives relative rates k_3/k_2 of $3.3(\pm 1.1) \times 10^{-5}$ and $(k_d + L)/k_2$ of $-2.3(\pm 3.5) \times 10^{11} \text{ cm}^{-3}$ (Table 2).

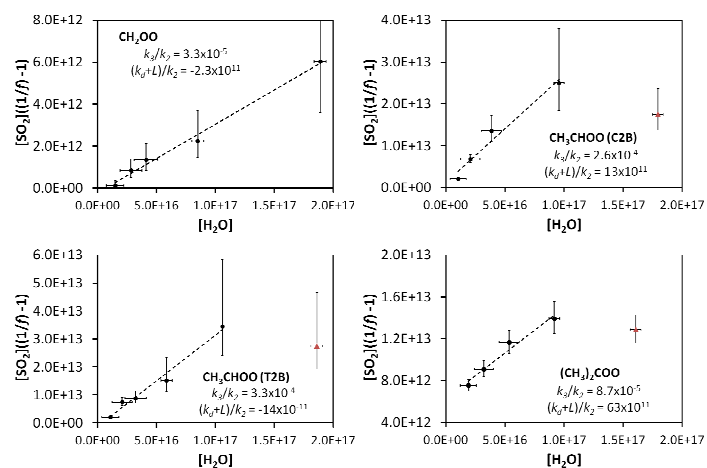


Figure 3 Application of Equation E3 to derive rate constants for reaction of CH_2OO , CH_3CHOO (derived from *cis*-but-2-ene; C2B), CH_3CHOO (derived from *trans*-but-2-ene; T2B), and $(\text{CH}_3)_2\text{COO}$ with H_2O (k_3) and decomposition (k_d), relative to that for reaction with SO_2 , k_3/k_2 and $(k_d+L)/k_2$ – see text.

These relative rates can be placed on an absolute basis using absolute measurements of $k_2(\text{SCI}+\text{SO}_2)$. In Table 3 we apply the absolute k_2 values reported by Welz *et al.*¹⁵, obtained using direct methods at reduced pressure (4 Torr), to the relative rates shown in Table 2. Using this method, the value obtained for $k_3(\text{CH}_2\text{OO}+\text{H}_2\text{O})$ is $1.3 (\pm 0.4) \times 10^{-15} \text{ cm}^3 \text{ s}^{-1}$. This is consistent with the recent determination by Welz *et al.*¹⁵, that $k_3 < 4 \times 10^{-15} \text{ cm}^3 \text{ s}^{-1}$, but is (*ca.* 14–50 times) greater than the recent estimates of Ouyang *et al.*¹⁸ ($k_3 = 2.5 (\pm 1) \times 10^{-17} \text{ cm}^3 \text{ s}^{-1}$) and Stone *et al.*¹⁷ ($k_3 < 9 \times 10^{-17} \text{ cm}^3 \text{ s}^{-1}$).

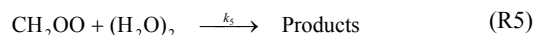
The derived (k_d+L) value for CH_2OO using this method is $-8.8 (\pm 13) \text{ s}^{-1}$, *i.e.* zero within uncertainty. Theoretical work²² has predicted $k_d(\text{CH}_2\text{OO})$ to be small ($\sim 0.3 \text{ s}^{-1}$), in agreement with the experimentally derived value reported here.

Table 2 SCI relative rate constants derived in this work using the single-SCI water monomer approach (*i.e.* Equation E3; see text). Uncertainty ranges ($\pm 2\sigma$, parentheses) indicate combined precision and systematic measurement error components.

SCI	10^5	10^{-11} cm^{-3}
	k_3/k_2	k_d/k_2
CH_2OO	3.3 (± 1.1)	-2.3 (± 3.5)
CH_3CHOO (C2B)	26 (± 10)	13 (± 43)
CH_3CHOO (T2B)	33 (± 10)	-14 (± 31)
$(\text{CH}_3)_2\text{COO}$	8.7 (± 2.5)	63 (± 14)

3.2.2 $\text{CH}_2\text{OO} + (\text{H}_2\text{O})_2$

Recent experimental work⁴⁶ has reported the reaction of CH_2OO with the water dimer, $(\text{H}_2\text{O})_2$, (Reaction R5) to be very fast ($1.1 \times 10^{-11} \text{ cm}^3 \text{ s}^{-1}$ – assuming $k_2 = 3.9 \times 10^{-11} \text{ cm}^3 \text{ s}^{-1}$ ¹⁵), in broad agreement with theoretical predictions⁴⁷, but in contrast to other experimental work⁴⁵.



The CH₂OO data from this study appear to be well described by a linear fit under the experimental conditions applied (a fast reaction of CH₂OO with (H₂O)₂ would be manifested as a significant upward curvature in Figure 3). However, this does not mean the results are inconsistent with reaction of CH₂OO with (H₂O)₂.

In Figure 4, Equation E4 (an expanded version of Equation E3, including the SCI + (H₂O)₂ reaction, R5) is applied to the data, now expressed in terms of (H₂O)₂, calculated for each RH via the equilibrium constant⁴⁸.

$$[SO_2]_0 \left(\frac{1}{f} - 1 \right) = \frac{k_3}{k_2} \sqrt{\frac{[(H_2O)_2]}{K_p}} + \frac{k_5}{k_2} [(H_2O)_2] + \frac{k_d}{k_2} \quad (\text{E4})$$

The value for k_3/k_2 (water monomer) derived from the fit shown in Figure 4 is $2.5 (\pm 0.7) \times 10^{-5}$. It is seen that this value is rather insensitive to the inclusion of the (H₂O)₂ term in Equation E4 as the value is within the uncertainties of the linear fit to the data presented in Figure 3 – see also Table 2. Adjusting this value to an absolute value for k_3 using the k_2 from Welz *et al.*¹⁵ gives $9.9 (\pm 2.9) \times 10^{-16} \text{ cm}^3 \text{ s}^{-1}$. The derived value of k_d/k_2 is $-6.4 (\pm 66) \times 10^{10} \text{ cm}^3$, which, using the Welz *et al.*¹⁵ k_2 gives an absolute value for k_d of $-1.5 (\pm 16) \text{ s}^{-1}$. This is again indistinguishable from zero, within uncertainty, as is the k_d determined from Equation E3 (Figure 3). Note the large uncertainties in k_d , resulting from allowing three parameters to vary in the optimisation; consequently k_d was fixed to zero in Equation E4 to determine the k_3/k_2 and k_5/k_2 values.

The derived value of k_5/k_2 (water dimer) is $1.4 (\pm 1.8) \times 10^{-2}$. Converting this to an absolute value for k_5 using the k_2 from Welz *et al.*¹⁵ gives $5.6 (\pm 7.0) \times 10^{-13} \text{ cm}^3 \text{ s}^{-1}$. This is roughly a factor of twenty smaller than the rate derived by Berndt *et al.*⁴⁶, but within a factor of two of the upper limit for k_5 deduced by Welz *et al.* ($< 3 \times 10^{-13} \text{ cm}^3 \text{ s}^{-1}$)⁴⁵ from the data presented by Stone *et al.*¹⁷. The inset plot in Figure 4 also shows two additional fits generated using Equation E4 with k_3/k_2 fixed to 9.9×10^{-16} and k_d fixed to zero. One fit line uses the k_5 value reported by Berndt *et al.*⁴⁶ (blue dashed line). This is seen to overestimate the presented data. The green dotted line shows a fit to the upper limits of the uncertainties of the measured data. This yields a k_5/k_2 value of $0.10 (\pm 0.01)$, giving a k_5 value of $3.9 (\pm 0.39) \times 10^{-12} \text{ cm}^3 \text{ s}^{-1}$.

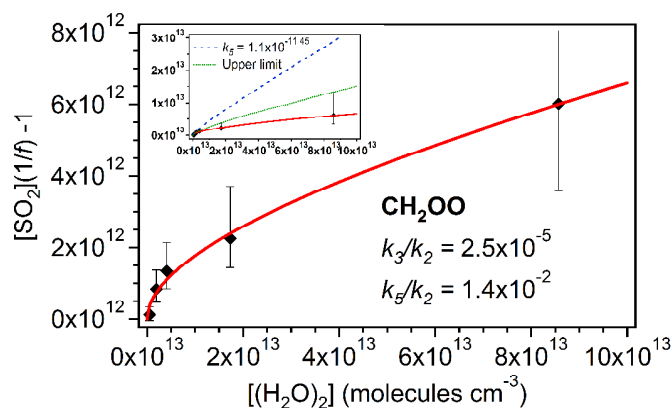


Figure 4 Application of Equation E4 to derive rate constants for reaction of CH₂OO with H₂O (k_3/k_2) and (H₂O)₂ (k_5/k_2) relative to that of CH₂OO with SO₂. Inset: Equation E4 as shown in the main figure (red line), E4 applied using the dimer reaction rate (k_5) reported by Berndt *et al.*⁴⁵ ($1.1 \times 10^{11} \text{ cm}^3 \text{ s}^{-1}$) (dashed line) and a fit of E4 to the upper limits of the uncertainties in the ethene data (solid green line).

The contribution of (H₂O)₂ to the removal of CH₂OO increases in relation to that of H₂O as [H₂O] increases. Hence at typical atmospheric [H₂O] ($\sim 2.5 - 7.5 \times 10^{17} \text{ molecules cm}^{-3}$), greater than was accessible in this study, reaction with (H₂O)₂ could become the dominant sink for CH₂OO. In this case using just the H₂O monomer kinetics in models would considerably underestimate the total effect of water on removal of CH₂OO in the atmosphere.

3.3 CH₃CHOO

3.3.1 Single SCI Approach

The CH₃CHOO data shown in Figure 3 for both *cis* and *trans*-but-2-ene appear to be well described (within the uncertainties) by a linear fit to Equation E3, with the exception of the experiment at the highest RH ([H₂O] = $1.8-1.9 \times 10^{17} \text{ cm}^{-3}$) in both cases. The kinetic parameters derived from a linear fit to the data (Figure 3), using Equation E3 (which treats the system as producing a single SCI), excluding the highest RH experiments, are shown in Table 2. Very similar results are obtained for k_3/k_2 for CH₃CHOO derived from both *cis*- and *trans*-but-2-ene ozonolysis, with values of $26 (\pm 10) \times 10^{-5}$ and $33 (\pm 10) \times 10^{-5}$ respectively. The $(k_d + L)/k_2$ obtained for CH₃CHOO from *cis*-but-2-ene ozonolysis is $13 (\pm 43) \times 10^{11} \text{ molecule cm}^{-3}$ and from *trans*-but-2-ene ozonolysis $-14 (\pm 31) \times 10^{11} \text{ molecule cm}^{-3}$. Berndt *et al.*³² reported the k_3/k_2 ratio from *trans*-but-2-ene ozonolysis to be $8.8 (\pm 0.4) \times 10^{-5}$ (also assuming a single SCI system), a factor of 3.75 smaller than that reported here.

The relative rate constants (Table 2) can be placed on an absolute basis using the absolute measurements of $k_2(\text{SCI}+\text{SO}_2)$ reported by Taatjes *et al.*¹⁶ (derived using the same methodology as for CH₂OO) (Table 3). As Equation E3 treats the SCI produced as a single SCI, we use an average of the *syn* and *anti* conformer rates presented in Taatjes *et al.*¹⁶, $4.55 \times 10^{-11} \text{ cm}^3 \text{ s}^{-1}$. Using this method, the value obtained for $k_3(\text{CH}_3\text{CHOO}+\text{H}_2\text{O})$ from *cis*-but-2-ene ozonolysis is $12 (\pm 4.5) \times 10^{-15} \text{ cm}^3 \text{ s}^{-1}$ and from *trans*-but-2-ene ozonolysis is $15 (\pm 4.5) \times 10^{-15} \text{ cm}^3 \text{ s}^{-1}$. Taking a mean of the k_3 values reported for the two CH₃CHOO conformers by Taatjes *et al.*¹⁶ gives a value of $7.0 \times 10^{-15} \text{ cm}^3 \text{ s}^{-1}$, while Sheps *et al.*⁴⁹ gives a mean value of $12 \times 10^{-15} \text{ cm}^3 \text{ s}^{-1}$. The values obtained for $(k_d + L)$ are $59 (\pm 196) \text{ s}^{-1}$ from *cis*-but-2-ene and $-64 (\pm 141) \text{ s}^{-1}$ from *trans*-but-2-ene. Clearly there is a large uncertainty associated with the k_d determined from this analysis. Fenske *et al.*²⁶ have reported $k_d(\text{CH}_3\text{CHOO})$ from *trans*-but-2-ene ozonolysis to be 76 s^{-1} (accurate to within a factor of three).

3.3.2 Two Conformer System

In Figure 1 it is evident that $d\text{SO}_2/d\text{O}_3$ falls rapidly with increasing [H₂O] for all but-2-ene experiments as RH is initially increased, but that the experiments at higher RH all appear to display a similar $d\text{SO}_2/d\text{O}_3$, *i.e.* the trend in decreasing SO₂ removal with increasing H₂O levels off. From this observation it appears that there may be competing H₂O dependencies to the SO₂ loss present. This is manifested in Figure 3 as a curving over of the data at high RH. We propose two possible explanations for this observation: firstly that it arises from differing kinetics of the two CH₃CHOO conformers formed in but-2-ene ozonolysis; secondly that the behaviour may reflect the presence of an additional oxidant being formed in the ozonolysis system that reacts with SO₂ but is less sensitive to H₂O. The first of these possibilities is discussed below, the second is discussed in relation to (CH₃)₂COO in the following section.

Table 3 Comparison of SCI relative rate constants derived in this work to relative and absolute values from the literature. Uncertainty ranges ($\pm 2\sigma$) indicate combined precision and systematic measurement error components.

SCI	10^5 k_3/k_2	10^{15} k_3 ($\text{cm}^3 \text{s}^{-1}$)	10^{-11} k_d/k_2 (cm^{-3})	k_d (s^{-1})	Reference	Method	Conditions ^a
CH ₂ OO	3.3 (± 1.1)	1.3 (± 0.4) ^b	-2.3 (± 3.5)	-8.8 (± 13) ^b	This work	Ethene Ozonolysis	298-303 K
		< 4			Welz <i>et al.</i> ¹⁵	Alkyl iodide photolysis	4 Torr 298 K
		< 0.09			Stone <i>et al.</i> ¹⁷	Alkyl iodide photolysis	200 Torr 295 K
CH ₃ CHOO	26 (± 10)	12 (± 4.5) ^c	13 (± 43)	59 (± 196) ^c	This work	C2B ozonolysis	296-302 K
	33 (± 10)	15 (± 4.5) ^c	-14 (± 31)	-64 (± 141) ^c	This work	T2B ozonolysis	297-302 K
		<i>anti</i> 10 (± 4) <i>syn</i> < 4			Taatjes <i>et al.</i> ¹⁶	Alkyl iodide photolysis	4 Torr 298 K
	8.8 (± 0.4)		12 (± 0.1)	76 (25-228)	Berndt <i>et al.</i> ³² Fenske <i>et al.</i> ²⁶	T2B ozonolysis T2B ozonolysis	293 K 296 K
(CH ₃) ₂ COO	8.7 (± 2.5)	2.1 (± 0.6) ^d	63 (± 14)	151 (± 35) ^d	This work	TME ozonolysis	298-299 K
	< 0.4		42 (± 3)		Berndt <i>et al.</i> ³²	TME ozonolysis	293 K

^a Experiments were conducted at atmospheric pressure unless stated otherwise.

^b Assuming $k_2 = 3.9 \times 10^{-11} \text{ cm}^3 \text{ s}^{-1}$ (Welz *et al.*¹⁵)

^c Assuming $k_2 = 4.55 \times 10^{-11} \text{ cm}^3 \text{ s}^{-1}$. Average of k_2 for *syn* and *anti* CH₃CHOO conformers from Taatjes *et al.*¹⁶

^d Assuming $k_2 = 2.4 \times 10^{-11} \text{ cm}^3 \text{ s}^{-1}$. k_2 for *syn*-CH₃CHOO from Taatjes *et al.*¹⁶

One explanation for the observed non-linearity at high RH apparent in Figure 3 is the differing reactivities of the *syn*- and *anti*-conformers of CH₃CHOO produced in the ozonolysis of *cis*- and *trans*-but-2-ene. It has been predicted⁵⁰ that the *anti*-conformer reacts with H₂O several orders of magnitude faster than the *syn*-conformer, while the rate constant for the SCI reaction with SO₂ has been determined experimentally¹⁶ to be about a factor of three greater for the *anti*-conformer than the *syn*-conformer. The fraction of each conformer that is lost to reaction with SO₂ can be considered in the same way as illustrated in Equation E2, leading to Equations E5 & E6 below, plus simplifications outlined in the following text. The total loss of SO₂ to CH₃CHOO is then the sum of the fractional loss to each conformer, multiplied by the relative SCI yield (γ) (*i.e.* ϕ^{syn} / ϕ) of that conformer (Equation E7).

$$f^{\text{syn}} = \frac{[\text{SO}_2]}{[\text{SO}_2] + \frac{k_3^{\text{syn}}}{k_2^{\text{syn}}}[\text{H}_2\text{O}] + \frac{k_d^{\text{syn}}}{k_2^{\text{syn}}}} \approx \frac{[\text{SO}_2]}{[\text{SO}_2] + \frac{k_d^{\text{syn}}}{k_2^{\text{syn}}}} \quad (\text{E5})$$

$$f^{\text{anti}} = \frac{[\text{SO}_2]}{[\text{SO}_2] + \frac{k_3^{\text{anti}}}{k_2^{\text{anti}}}[\text{H}_2\text{O}] + \frac{k_d^{\text{anti}}}{k_2^{\text{anti}}}} \approx \frac{[\text{SO}_2]}{[\text{SO}_2] + \frac{k_3^{\text{anti}}}{k_2^{\text{anti}}}[\text{H}_2\text{O}]} \quad (\text{E6})$$

$$f = \gamma^{\text{syn}} f^{\text{syn}} + \gamma^{\text{anti}} f^{\text{anti}} \quad (\text{E7})$$

Equation E8 can then be fitted to the data presented in Figure 3 for *cis*- and *trans*-but-2-ene (Figure 5).

$$[\text{SO}_2] \left(\frac{1}{f} - 1 \right) = [\text{SO}_2] \left(\frac{1}{\gamma^{\text{syn}} f^{\text{syn}} + \gamma^{\text{anti}} f^{\text{anti}}} - 1 \right) \quad (\text{E8})$$

Here we make two assumptions to reduce the degrees of freedom and hence make the problem tractable with the dataset available. First it is assumed that $k_3^{\text{syn}}[\text{H}_2\text{O}]$ may be neglected, in keeping with theoretical predictions²⁴ predicting k_d^{syn} to be over three orders of magnitude greater than $k_3^{\text{syn}}[\text{H}_2\text{O}]$. Further theoretical work⁵⁰ predicts a rate constant for *syn*-CH₃CHOO+H₂O of $2.39 \times 10^{-18} \text{ cm}^3 \text{ s}^{-1}$, and recent experimental work⁴⁹ yields an upper limit for k_3^{syn} of $< 2 \times 10^{-16} \text{ cm}^3 \text{ s}^{-1}$. Hence with k_d^{syn} expected to be relatively fast, given the decomposition rate presented here for (CH₃)₂COO (a *syn*-conformer) and the facile decomposition route available via the hydroperoxide mechanism for the *syn*-conformer, it can be assumed that $k_d^{\text{syn}} \gg k_3^{\text{syn}}[\text{H}_2\text{O}]$ at the experimental conditions reported here. Second it is assumed that $k_d^{\text{anti}} \ll k_3^{\text{anti}}[\text{H}_2\text{O}]$ under the experimental conditions used. If the kinetics derived from treating the but-2-ene data in Figure 3 as representing a single SCI are dominated by the *anti*-conformer then the k_d derived from these kinetics, which is indistinguishable from zero within the uncertainties, suggests that k_d^{anti} is small. Taatjes *et al.*¹⁶ report k_3^{anti} to be $1.0 (\pm 0.4) \times 10^{-14} \text{ cm}^3 \text{ s}^{-1}$, while Sheps *et al.*⁴⁹ report a value of $2.4 (\pm 0.4) \times 10^{-14} \text{ cm}^3 \text{ s}^{-1}$. Thus, even at the lowest [H₂O] considered here ($\sim 1 \times 10^{16} \text{ cm}^{-3}$), loss of *anti*-CH₃CHOO to H₂O would be $> 100 \text{ s}^{-1}$, and decomposition negligible in comparison (including a k_d^{anti} of 50 s^{-1} only changes the derived k_3^{anti} and k_d^{syn} values by $< 5\%$).

Fitting Equation E8 to the data shown in Figure 5 derives a range of values for k_3^{anti} and k_d^{syn} dependent on the values of γ^{anti} and γ^{syn} used. As the CIs, once formed and thermalised, are expected to show the same kinetic behaviour irrespective of their precursor alkene, the measurements from the *cis*-but-2-ene and *trans*-but-2-ene experiments can be used in combination to constrain k_3^{anti} , k_d^{syn} and also γ^{syn} and γ^{anti} from each alkene. Figure 6 plots the k_3^{anti} vs. k_d^{syn} determined at different γ^{syn} and γ^{anti} from *cis*-but-2-ene and *trans*-but-2-ene. Where these two lines intercept represents the unique solution for both k_3^{anti} and k_d^{syn} and for γ^{syn} and γ^{anti} (Table 4).

Table 4 Kinetic parameters derived for *syn*-CH₃CHOO and *anti*-CH₃CHOO from two-component fits to the *trans*-but-2-ene (T2B) and *cis*-but-2-ene (C2B) experiments (see Figure 5). Also relative (γ) and absolute (ϕ) yields of the two conformers.

CH ₃ CHOO	10 ⁴		10 ¹⁴		10 ⁻¹³		k_d (s ⁻¹)		γ^a		ϕ		Reference	Conditions ^b
	k_3/k_2	k_3 (cm ³ s ⁻¹)	k_3 (cm ³ s ⁻¹)	k_d/k_2 (cm ³)	T2B	C2B	T2B	C2B						
<i>syn</i>	-	-	-	1.2 (\pm 1.1)	288 (\pm 275)	0.25	0.45	0.07	0.17	This work	-			
		< 0.4								Taatjes <i>et al.</i> ¹⁶	4 Torr			
		< 0.02								Sheps <i>et al.</i> ⁴⁹	200 Torr			
					20 (3-30)					Novelli <i>et al.</i> ²³	735 Torr			
<i>anti</i>	3.5 (\pm 3.1)	2.3 (\pm 2.1)	-	-	-	0.75	0.55	0.21	0.21	This work	-			
		1.0 (\pm 0.4)								Taatjes <i>et al.</i> ¹⁶	4 Torr			
		2.4 (\pm 0.4)								Sheps <i>et al.</i> ⁴⁹	200 Torr			

^a $\gamma^{syn} = \phi^{syn} / \phi$.

^b Experiments were conducted at atmospheric pressure unless stated otherwise and temperatures from 293 to 303 K.

Figure 6 determines k_3^{anti}/k_2^{anti} to be $3.5 (\pm 3.1) \times 10^{-4}$ and k_d^{syn}/k_2^{syn} to be $1.2 (\pm 1.1) \times 10^{13} \text{ cm}^{-3}$. The 2σ uncertainties presented are, unsurprisingly, large as there are two free parameters. Using the relevant values of k_2 for the *syn* and *anti*-CH₃CHOO conformers from Taatjes *et al.*¹⁶ to place the relative rate constants on an absolute basis gives a value for k_3^{anti} of $2.3 (\pm 2.1) \times 10^{-14} \text{ cm}^3 \text{ s}^{-1}$ and for k_d^{syn} of $288 (\pm 275) \text{ s}^{-1}$. This k_3^{anti} is comparable to (a factor of two greater than) that reported by Taatjes *et al.*¹⁶ ($1.0 (\pm 0.4) \times 10^{-14}$). Novelli *et al.*²³ have recently reported k_d^{syn} to be an order of magnitude smaller ($3\text{-}30 \text{ s}^{-1}$) based on direct observation of OH formation during *trans*-but-2-ene ozonolysis at atmospheric pressure.

The point of interception in Figure 6 also determines the relative yields of the two conformers, γ^{syn} and γ^{anti} (which in turn has been used to derive the optimised fits shown in Figure 5). For *cis*-but-2-ene these are determined as 0.45 and 0.55 for γ^{syn} and γ^{anti} respectively. For *trans*-but-2-ene they are determined as 0.25 for γ^{syn} and 0.75 for γ^{anti} . The analysis performed in this section has implications for the determination of the SCI yield. Using the relative rate constant k_3/k_2 (*anti*-CH₃CHOO) obtained, as shown in Table 4, it is calculated that $\sim 90\%$ of the *anti*-CH₃CHOO produced in the SCI yield experiments would react with SO₂. From the determined k_d/k_2 (*syn*-CH₃CHOO) it is calculated that $\sim 67\%$ of the *syn*-CH₃CHOO produced in the SCI yield experiments would react with SO₂. Applying these (with the corresponding *syn* and *anti* yields shown in Table 4) corrections to ϕ_{min} determines total SCI yields of 0.29 for *trans*-but-2-ene and 0.42 for *cis*-but-2-ene. These values both lie within the uncertainties in the SCI yields presented in Table 1 for the two but-2-ene systems.

It is not practicable to assess the possible contribution of the water dimer to the SCI loss for CH₃CHOO because of the number of free parameters that would result for a small dataset. However, theoretical predictions⁴⁷ suggest that this may be less important for CH₃CHOO than for CH₂OO, indicating $k(\text{H}_2\text{O}_2)/k(\text{H}_2\text{O})$ to be two orders of magnitude smaller for *anti*-CH₃CHOO than for CH₂OO.

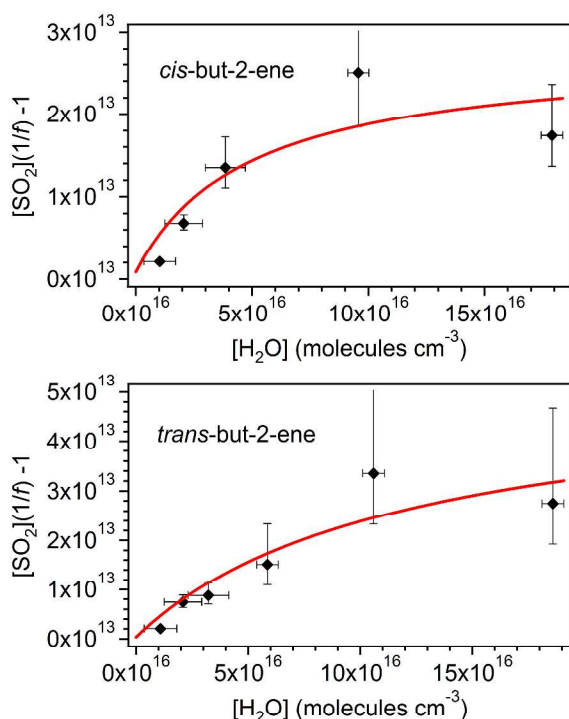


Figure 5 Fits of Equation E8 to the *cis*-but-2-ene and *trans*-but-2-ene data shown in Figure 3. γ^{syn} and γ^{anti} are 0.45 and 0.55 for *cis*-but-2-ene and 0.25 and 0.75 for *trans*-but-2-ene (see Figure 6).

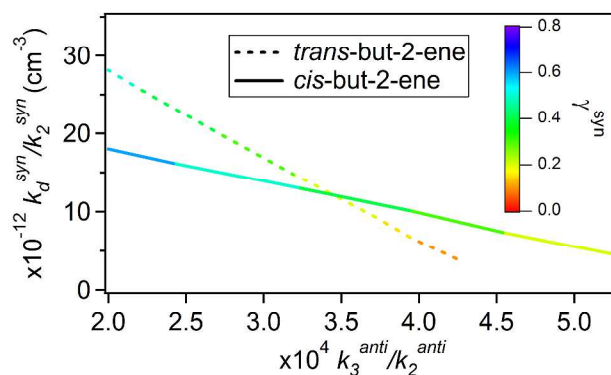


Figure 6 The ranges of k_3^{anti}/k_2^{anti} and k_d^{syn}/k_2^{syn} determined from fitting Equation E8 to the but-2-ene data (Figure 5). The colour legend shows the fraction of the total CH₃CHOO formed that is *syn*-CH₃CHOO (γ^{syn}).

3.4 (CH₃)₂COO

3.4.1 Linear Fit

For (CH₃)₂COO a value of $8.7 (\pm 2.5) \times 10^{-5}$ (Table 2) was obtained from a linear fit to the data in Figure 3, excluding the experiment performed at the highest RH ([H₂O] = 1.6×10^{17} cm⁻³) from the regression. $(k_d+L)/k_2$ for (CH₃)₂COO was determined as $63 (\pm 14) \times 10^{11}$ molecule cm⁻³. These values can be placed on an absolute basis using the absolute measurements of $k_2(\text{syn-CH}_3\text{CHOO}+\text{SO}_2)$ reported by Taatjes *et al.*¹⁶ as there are no reported k_2 values from direct experiments and (CH₃)₂COO is a *syn*-conformer (*i.e.* there is always a methyl group in a *syn* orientation to the terminal oxygen). This gives values for k_3 ((CH₃)₂COO + H₂O) of $2.1 (\pm 0.6) \times 10^{-15}$ cm³ s⁻¹ and for k_d of $151 (\pm 35)$ s⁻¹ (Table 3).

Berndt *et al.*³² have recently reported the k_3/k_2 ratio for (CH₃)₂COO to be $< 0.4 \times 10^{-5}$ (*i.e.* approximately a factor of 22 lower than the relative rate reported in this study). Theoretical predictions⁵⁰ also suggest k_3 to be very slow, 3.9×10^{-17} cm³ s⁻¹. No measured values have been reported for k_d ((CH₃)₂COO), but a more facile overall decomposition than for CH₂OO or the mean of CH₃CHOO might be anticipated as the vinyl-hydroperoxide isomerisation channel²⁶ is always available.

3.4.2 Additional Oxidant

In the case of the SCI formed from TME ozonolysis, (CH₃)₂COO, there is always a methyl group in a *syn* position to the carbonyl oxide moiety, thus the analysis presented in Section 3.3.2 for the CH₃CHOO isomers does not apply. A possible alternative explanation for the observed behaviour (and possible contributor to the behaviour observed in the but-2-ene systems) is that there is a further oxidant (X) of SO₂, in addition to the SCI, being formed during the ozonolysis reaction. If this oxidant reacts relatively slowly with H₂O, it could give rise to the apparent ‘two component’ nature of the observations seen in Figure 3. It may also provide an alternative explanation of the observed nature of the SO₂ loss from the but-2-ene experiments or could be occurring in addition to the effects of differing conformer reactivities.

Equation E9 (below) is an expanded version of E2, in which we consider the contribution from a second SO₂ oxidant, making the approximation that this species does not react appreciably with water vapour. In Equation E9, f is the sum of f^{SCI} (the fraction of SCI reacting with SO₂) and f^x , each multiplied by the relative amount of the total oxidant (*i.e.* SCI + X) γ^{SCI} and γ^x . Following the assumption of negligible H₂O reactivity, $(d\text{SO}_2/d\text{O}_3)_x$ in Equation E9 can be derived from the SO₂ loss at the highest RH experiments (*i.e.* when all the SO₂ loss is attributed to X+SO₂) is ~ 10 ppbv. Therefore, loss of SO₂ from reaction with X, relative to the loss of O₃ $(d\text{SO}_2/d\text{O}_3)_x$ is approximately 0.025. ϕ represents the total oxidants formed (*i.e.* $\phi_{\text{SCI}} + \phi_x$). Assuming that γ^x is not dominant (< 0.5), then ϕ , as calculated from correcting ϕ_{min} as in Section 3.1, changes little (0.31 – 0.34) from the value presented in Table 1. Equation E10 is then an expanded version of Equation E3 that includes the additional oxidant term.

$$f = \gamma^{\text{SCI}} f^{\text{SCI}} + \gamma^x f^x = \gamma^{\text{SCI}} f^{\text{SCI}} + \frac{1}{\phi} \left(\frac{d\text{SO}_2}{d\text{O}_3} \right)_x \quad (\text{E9})$$

$$[\text{SO}_2] \left(\frac{1}{f} - 1 \right) = [\text{SO}_2] \left[\left(\frac{\gamma^{\text{SCI}} [\text{SO}_2]}{[\text{SO}_2] + \frac{k_3}{k_2} [\text{H}_2\text{O}] + \frac{k_d}{k_2}} + \frac{1}{\phi} \left(\frac{d\text{SO}_2}{d\text{O}_3} \right)_x \right)^{-1} - 1 \right] \quad (\text{E10})$$

Figure 7 shows Equation E10 fitted to the TME data from Figure 3. It is not possible to determine unique values for the parameters included in Equation E10 due to the degrees of freedom vs. the limited data set. The fit shown in Figure 7 uses values of $\phi = 0.34$, $\gamma^{\text{SCI}} = 0.88$, $k_3/k_2 = 6.7 \times 10^{-4}$ and $k_d/k_2 = 1.2 \times 10^{12}$ cm⁻³. However, Figure 7 does demonstrate that a two-oxidant system, as represented by Equation E10, is able to describe the data within uncertainty.

Figure 7 also includes linear fit (*i.e.* Equation E3) to the full (CH₃)₂COO dataset (including the highest RH experiment). While it seems unlikely that the curvature observed in the measurements is a result of measurement error (as described in Section 3.1), this must be considered as a possibility for (CH₃)₂COO in light of the two conformer explanation not being applicable. The linear fit in Figure 7 gives a k_3/k_2 value of $3.8 (\pm 3.2) \times 10^{-5}$ cm³ s⁻¹, a factor of two smaller than the k_3/k_2 value presented in Table 2.

The most obvious candidate for an additional oxidant present to consume SO₂ is OH. OH radicals are produced in the chamber, primarily (in the absence of sunlight and NO_x) through the alkene + ozone reaction¹¹. However cyclohexane was added in excess at the beginning of each experiment to act as an OH scavenger, such that SO₂ reaction with OH was calculated to be $\leq 1\%$ of the total

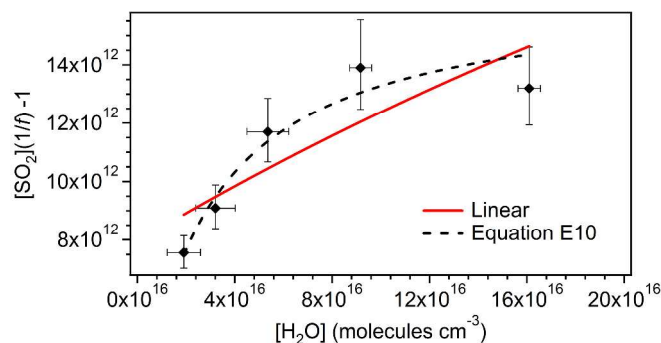


Figure 7 Fitting Equation E9 to the TME data shown in Figure 3. Also applying a linear fit to the full dataset.

chemical SO₂ removal in all experiments. Other potential candidates for this oxidant species include the (stabilised) vinyl hydroperoxide (VHP) intermediate, a secondary ozonide (formed through an SO₂ – SCI cyclic adduct), and dioxirane (Scheme 1).

Drozd *et al.*¹⁰ have presented evidence for substantial VHP stabilisation (derived from the (CH₃)₂COO CI) at pressures of a few hundred Torr, with a lifetime of the order of a few hundred milliseconds with respect to decomposition to form OH, providing scope for bimolecular reactions of this species to occur. This would be consistent with the kinetic observations presented here: a small yield in the systems with *syn*-SCIs, while for ethene, no VHP intermediate is available, and the standard chemistry (R1 – R4) can be used to satisfactorily reproduce the observations. However, no significant SO₂ reactivity is known for the peroxide or alkene functionalities present in the closed shell VHP in isolation, hence it may be surprising if this species reacted rapidly with SO₂, although theoretical studies have suggested that the VHP may react with H₂O²³.

Secondary ozonide species, formed as an adduct from the SCI + SO₂ reaction, have been suggested to account for the observed isotopic exchange in alkene-ozone-SO₂ systems²⁵, and are suggested to have lifetimes of seconds or longer.¹⁹ Such a secondary ozonide could react with a further SO₂ molecule (*i.e.* a two-component secondary ozonide catalysed oxidation route for SO₂ to SO₃ conversion), however a substantial humidity dependence to the

overall process may still be anticipated (on the basis of SCI removal through the SCI + H₂O reaction), which is not observed here.

The 'hot acid/ester channel' (rearrangement and decomposition via a dioxirane intermediate) is the dominant isomerisation route available for *anti*-SCIs. Although the hydroperoxide channel is the principal isomerisation route for *syn*-SCIs, the ester mechanism is also available²⁵, and it is likely that a small proportion of the *syn*-CI will isomerise through this channel to form a dioxirane. Dioxiranes are known to be highly reactive and selective oxidising agents^{51,52}, and have a particular affinity for sulphur compounds⁵³. Additional oxidation of SO₂ by the dioxirane, over and above that arising directly from reaction with the SCI, could then explain the observed behaviour of SO₂ in the TME experiments (and contribute to the behaviour observed for the but-2-ene systems). For the small CI CH₂OO, formed in the ethene system, it has been predicted that the dioxirane formed is considerably less stable than the methyl substituted dioxiranes formed from but-2-ene and TME ozonolysis, and furthermore will decompose promptly due to chemical activation.

The possibility of non-CI products of the ozonolysis system being responsible for some of the observed SO₂ oxidation has been suggested previously as an alternative (or additional) explanation for the observed behaviour of SO₂ in the atmosphere^{1,54,55}. In their laboratory study Berndt *et al.*¹⁹ note that their data were not perfectly described by a model in which a single (SCI related) SO₂ oxidation process was assumed, and commented that the SO₂ oxidation in ozonolysis systems may in fact be more complex. Taatjes *et al.*⁵⁶ have recently suggested that these data¹⁹ are consistent with a two-component oxidation system, either two processes removing SO₂ in parallel (as described above), or through a sequential two-step SO₂ removal mechanism, such as the secondary ozonide route outlined above. However, this latter mechanism cannot (in isolation) account for the observations presented here.

The presence of an additional oxidant would have implications for the role of alkene ozonolysis in oxidation of trace gases in the atmosphere. If an oxidant is being formed that reacts slowly with H₂O then this, perhaps in addition to SCI, may contribute to the additional (non-OH) SO₂ oxidation observed in recent field experiments¹. Further investigation of this possibility is needed.

As for CH₃CHOO, the analysis performed in this section has implications for the determination of the SCI ((CH₃)₂COO) yield. Using the value of k_d derived from the linear fit to all the data shown in Figure 7 would indicate an SCI yield of 0.33. Using the value of k_d derived from the 'additional oxidant fit in Figure 7, and taking into account that ~10 ppb of the SO₂ loss in the high SO₂ experiment would be attributed to reaction with the additional oxidant rather than the SCI, determines a slightly lower ϕ_{\min} of 0.23, and a corrected yield of 0.32, very similar to that shown in Table 1. Both of these possible alternative SCI yields lie within the uncertainties in the SCI yield from TME ozonolysis presented in Table 1.

As for CH₃CHOO, it is not possible to quantitatively consider the contribution of the water dimer to the SCI loss given the limited data, but theory⁵³ predicts $k(\text{H}_2\text{O})_2/k(\text{H}_2\text{O})$ to be three orders of magnitude smaller than that for CH₂OO suggesting that reaction with the water dimer would be unimportant for (CH₃)₂COO at typical atmospheric boundary layer [H₂O].

4. Atmospheric Implications

The derived values for k_3 reported in Table 3 correspond to loss rates for reaction of SCI with H₂O in the atmosphere of 650 s⁻¹ for CH₂OO, ~3500 s⁻¹ for CH₃CHOO and ~1050 s⁻¹ for (CH₃)₂COO (assuming [H₂O] = 5 × 10¹⁷ molecules cm⁻³, equivalent to an RH of

65% at 298 K). Comparing this to the derived k_d values it is seen that reaction with H₂O is predicted to be the main sink for SCI in the atmosphere, but also that loss through decomposition cannot be neglected for some SCIs – contributing on the order of 0-1 % for CH₃CHOO and 13% for (CH₃)₂COO.

An estimate of a mean steady state SCI concentration in the background atmospheric boundary layer can then be calculated using Equation E11.

$$[SCI] = \frac{[Alkene][O_3]k_1\phi}{k_3[H_2O] + k_d} \quad (\text{E11})$$

Using the data given below, a steady state SCI concentration of 1.7 × 10³ molecules cm⁻³ is estimated for an ozonolysis source (noting that other potential atmospheric sources of SCI exist, *e.g.* photolysis of alkyl-iodides in the marine boundary layer, and sinks, *e.g.* reaction with NO and NO₂). This assumes an ozone mixing ratio of 40 ppbv, an alkene mixing ratio of 2 ppbv, ϕ of 0.35, and mean reaction rate constants k_1 (alkene – ozone) of 1 × 10⁻¹⁶ cm³ s⁻¹, k_2 (SCI + SO₂) of 3.5 × 10⁻¹¹ cm³ s⁻¹, k_3 (SCI + H₂O) of 2 × 10⁻¹⁵ cm³ s⁻¹, k_d of 30 s⁻¹ with [H₂O] of 5 × 10¹⁷ cm⁻³ (RH ~ 65 %).

However, in the case of CH₃CHOO the data shown in Figure 3, and the discussion above, indicate contributions from multiple species – *syn*- and *anti*-conformers with contrasting behaviour. It is clear that the burden of CH₃CHOO in the atmosphere would be better described by considering these two fractions of SO₂ loss separately. Equation E12 expands Equation E11 to treat the two conformers separately, where [SCI] = [*anti*-SCI] + [*syn*-SCI], making the same assumptions as for the analysis of CH₃CHOO in Equations E5 and E6. k_3^{anti} is estimated to be 1 × 10⁻¹⁴ cm³ s⁻¹ (taking into account that CH₂OO is considered as an *anti*-SCI in this analysis and that the derived $k_3(\text{CH}_2\text{OO})$ is more than an order of magnitude smaller than the derived $k_3(\text{CH}_3\text{CHOO})$ of 2.3 × 10⁻¹⁴ cm³ s⁻¹), k_d^{syn} is assumed to be 200 s⁻¹ and $\phi^{anti} = \phi^{syn} = 0.175$. Additionally the *anti*-SCI + water dimer reaction is also considered, using a value of 5.6 × 10⁻¹³ cm³ s⁻¹ as derived for CH₂OO in this work.

$$[SCI] = [Alkene][O_3]k_1 \left(\frac{\phi^{anti}}{k_3^{anti}[H_2O] + k_5^{anti}K_p[H_2O]^2} + \frac{\phi^{syn}}{k_d^{syn}} \right) \quad (\text{E12})$$

Using these values in Equation E12 determines [*anti*-SCI] = 164 molecules cm⁻³ and [*syn*-SCI] = 4.4 × 10³ molecules cm⁻³. The formation of an additional oxidant during alkene ozonolysis would be expected to have a similar effect to the two component contribution presented in Equation E12 based on the apparent yields from the experiments presented here. From this analysis the atmospheric SCI burden is seen to likely be dominated by *syn*-SCI since this term is at least an order of magnitude greater than the *anti*-SCI term.

A typical diurnal loss rate of SO₂ to OH ($k_{OH} \times [\text{OH}]$) is 9 × 10⁻⁷ s⁻¹¹⁵, while the SO₂ loss rate due to reaction with SCI, using the values derived from Equation E12, would be 1.2 × 10⁻⁷ s⁻¹. This suggests, for the conditions and assumptions given above, the loss of SO₂ to SCI to be about 13 % of loss to OH. This analysis neglects additional chemical sinks for SCI, which would reduce SCI abundance but are unlikely to be competitive with the two main SCI loss processes identified herein. SCI concentrations are expected to vary greatly depending on the local environment, *e.g.* alkene abundance may be considerably higher (and with a different reactive mix of alkenes) in a forested environment, compared to a rural background environment. The majority of the SCI burden, particularly in forested regions, is likely to be dominated by larger

SCI derived from (C₅) isoprene and (C₁₀) monoterpenes. The chemistry of these species could differ greatly from the small SCI reported here (which we have found to be structure specific, even for small alkene systems), especially for tethered SCI derived from ozonolysis of internal double bonds within (for example) some monoterpenes. It is clear that the total SCI loss rate is dependent upon SCI identity and configuration, and that further work is required to quantify speciated SCI in the atmosphere, and to accurately calculate SCI concentrations for use in atmospheric modelling.

5. Conclusions

It has been shown that at relatively low [H₂O] (< 1 × 10¹⁷ cm⁻³) the loss of SO₂ in the presence of four ozone-alkene systems: ethene, *cis*-but-2-ene, *trans*-but-2-ene and 2,3-dimethyl-but-2-ene significantly decreases with increasing water vapour. This is consistent with production of a stabilised Criegee intermediate from the ozonolysis reaction and subsequent reaction of this species with SO₂ and H₂O. Competition between H₂O and SO₂ for reaction with the SCI leads to the observed relationship which is sensitive to water vapour abundance over a relatively narrow range of RH. Derived kinetic data for these ozonolysis systems shows that the reaction rates are dependent on the structure of the SCI. At [H₂O] > 1 × 10¹⁷ cm⁻³ the SO₂ loss in the presence of *cis*- and *trans*-but-2-ene, and 2,3-dimethyl-but-2-ene appears to show a reduced dependence upon H₂O. The results suggest that there is an H₂O dependent and an H₂O independent fraction to the observed SO₂ loss in these systems. These two fractions may be attributable to differing kinetics of the two conformers produced in but-2-ene ozonolysis or to other oxidant products of the alkene ozonolysis reaction. This observation means that SCI structure must be considered in atmospheric modelling of SCI production from alkene ozonolysis, and suggests that the atmospheric SCI burden (and hence the oxidation of trace gases) will be dominated by *syn*-SCI.

This work provides constraints on the behaviour of SCI formed through alkene ozonolysis under conditions relevant to the atmospheric boundary layer, but also highlights the complex nature and incomplete current understanding of the ozonolysis system. Further research is needed to definitively quantify the impact of this chemistry upon atmospheric oxidation.

Acknowledgements

The assistance of the EUPHORE staff is gratefully acknowledged. Marie Camredon, Stephanie La and Mat Evans are thanked for helpful discussions. This work was funded by EU FP7 EUROCHAMP 2 Transnational Access activity (E2-2012- 05-28-0077), the UK NERC (NE/K005448/1) and Fundacion CEAM. Fundación CEAM is partly supported by Generalitat Valenciana, and the projects GRACCIE (Consolider-Ingenio 2010) and FEEDBACKS (Prometeo - Generalitat Valenciana). EUPHORE instrumentation is partly funded by the Spanish Ministry of Science and Innovation, through INNPLANTA project: PCT-440000-2010-003. LV is supported by the Max Planck Graduate Center with the Johannes Gutenberg-Universität Mainz (MPGC).

Notes and references

- R. L. Mauldin III, T. Berndt, M. Sipilä, P. Paasonen, T. Petäjä, S. Kim, T. Kurtén, F. Stratmann, V. -M. Kerminen and M. Kulmala, *Nature*, 2012, **488**, 193.
- G. Sarwar, K. Fahey, R. Kwok, R. C. Gilliam, S. J. Roselle, R. Mathur, J. Xue, J. Yu and W. P. L. Carter, *Atmos. Environ.*, 2013, **68**, 186
- P. Forster and V. Ramaswamy et al, *In Chap. 2, IPCC 4*, 2007, 160
- R. A. Cox and S. A. Penkett, *Nature*, 1971, **230**, 321
- R. Criegee and G. Wenner, *Liebigs. Ann. Chem.*, 1949, **564**, 9.
- D. Johnson and G. Marston, *Chem. Soc. Rev.*, 2008, **37**, 699.
- H. Niki, P. D. Maker, C. M. Savage, L. P. Breitenbach, and M. D. Hurley, *J. Phys. Chem.*, 1987, **91**, 941 .
- R. I. Martinez and J. T. Herron, *J. Phys. Chem.*, 1987, **91**, 946
- G. T. Drozd, J. Kroll and N. M Donahue, *J. Phys. Chem. A*, 2011, **115**, 161.
- G. T. Drozd and N. M Donahue, *J. Phys. Chem. A*, 2011, **115**, 4381.
- M. S. Alam, A. R. Rickard, M. Camredon, K. P. Wyche, T. Carr, K. E. Hornsby, P. S. Monks and W. J. Bloss, *J. Phys. Chem. A*, 2013, **117**, 12468
- K. Izumi, M. Mizuochi, K. Murano and T. Fukuyama, *Atmos. Environ.*, 1987, **21**, 1541.
- Calvert, J. G., R. Atkinson, J. A. Kerr, S. Madronich, G. K. Moortgat, T. J. Wallington and G. Yarwood, *Oxford University Press*, New York, 2000.
- C. A. Taatjes, G. Meloni, T. M. Selby, A. J. Trevitt, D. L. Osborn, C. J. Percival, D. E. Shallcross, *J. Am. Chem. Soc.*, 2008, **130**, 11883
- O. Welz, J. D. Savee, D. L. Osborn, S. S. Vasu, C. J. Percival, D. E. Shallcross, and C. A. Taatjes, *Science*, 2012, **335**, 204.
- C. A. Taatjes, O. Welz, A. J. Eskola, J. D. Savee, A. M. Scheer, D. E. Shallcross, B. Rotavera, E. P. F. Lee, J. M. Dyke, D. W. K. Mok, D. L. Osborn and C. J. Percival, *Science*, 2013, **340**, 177.
- D. Stone, M. Blitz, L. Daubney, N. U. M. Howes and P. Seakins, *Phys. Chem. Chem. Phys.*, 2014, **16**, 1139
- B. Ouyang, M. W. McLeod, R. L. Jones and W. J. Bloss, *Phys. Chem. Chem. Phys.*, 2013, **15**, 17070.
- T. Berndt, T. Jokinen, R. L. Mauldin III, T. Petaja, H. Herrmann, H. Junninen, P. Paasonen, D. R. Worsnop and M. Sipilä, *J. Phys. Chem. Lett.*, 2012, **3**, 2892.
- L. Vereecken, H. Harder and A. Novelli, *Phys. Chem. Chem. Phys.*, 2012, **14**, 14682.
- J. R. Pierce, M. J. Evans, C. E. Scott, S. D. D'Andrea, D. K. Farmer, E. Swietlicki and D. V. Spracklen, *Atmos. Chem. Phys.*, 2013, **13**, 3163.
- M. Olzmann, E. Kraka, D. Cremer, R. Gutbrod and S. Andersson, *J. Phys. Chem. A*, 1997, **101**, 9421.
- A. Novelli, L. Vereecken, J. Lelieveld and H. Harder, *Phys. Chem. Chem. Phys.*, 2014, DOI: 10.1039/C4CP02719A.
- K. T. Kuwata, M. R. Hermes, M. J. Carlson and C. K. Zogg, *J. Phys. Chem. A*, 2010, **114**, 9192.
- J. T. Herron, R. I. Martinez and R. E. Huie, *Int. J. Chem. Kinet.*, 1982, **14**, 201.
- J. D. Fenske, A. S. Hasson, A. W. Ho and S. E. Paulson, *J. Phys. Chem. A*, 2000, **104**, 9921.
- J. H. Kroll, S. R. Sahay, J. G. Anderson, K. L. Demerjian and N. M. Donahue, *J. Phys. Chem. A*, 2001, **105**, 4446.
- J. M. Beames, F. Liu, L. Lu and M. I. Lester, *J. Am. Chem. Soc.*, 2012, **134**, 19104.
- J. M. Beames, F. Liu, L. Lu and M. I. Lester, *J. Chem. Phys.*, 2013, **138**, 244307.
- K. H. Becker, EUPHORE: Final Report to the European Commission, Contract EV5V-CT92-0059, Bergische Universität Wuppertal, Germany, 1996.
- M. S. Alam, M. Camredon, A. R. Rickard, T. Carr, K. P. Wyche, K. E. Hornsby, P. S. Monks and W. J. Bloss, *Phys. Chem. Chem. Phys.*, 2011, **13**, 11002.
- T. Berndt, T. Jokinen, M. Sipilä, R. L. Mauldin, H. Herrmann, F. Stratmann, H. Junninen, and M. Kulmala, *Atmos. Environ.*, 2014, **89**, 603.
- S. M. Saunders, M. E. Jenkin, R. G. Derwent and M. J. Pilling, *Atmos. Chem. Phys.*, 2003, **3**, 161.

- 34 H. Niki, P. D. Maker, C. M. Savage and L. P. Breitenbach, *J. Phys. Chem.*, 1981, **85**, 1024.
- 35 S. Hatakeyama, H. Kobayashi and H. Akimoto, *J. Phys. Chem.*, 1984, **88**, 4736.
- 36 O. Horie and G. K. Moortgat, *Atmos. Environ. Part A*, 1991, **24**, 1881.
- 37 P. Neeb, O. Horie and G. K. Moortgat, *Int. J. Chem. Kinet.*, 1996, **28**, 721.
- 38 A. S. Hasson, G. Orzechowska and S. E. Paulson, *J. Geophys. Res.*, 2001, **106**, 34131.
- 39 A. R. Rickard, D. Johnson, C. D. McGill and G. Marston, *J. Phys. Chem. A*, 1999, **103**, 7656.
- 40 H. Niki, P. D. Maker, C. M. Savage and L. P. Breitenbach, *Chem. Phys. Letts.*, 1977, **46**, 327.
- 41 R. A. Cox and S. A. Penkett, *J. Chem. Soc. Faraday. Trans.*, 1972, **68**, 1735.
- 42 H. G. Kjaergaard, T. Kurtén, L. B. Nielsen, S. Jørgensen and P. O. Wennberg, *J. Phys. Chem. Lett.*, 2013, **4**, 2525.
- 43 L. Vereecken, H. Harder and A. Novelli, *Phys. Chem. Chem. Phys.*, 2014, **16**, 4039.
- 44 C. A. Taatjes, O. Welz, A. J. Eskola, J. D. Savee, D. L. Osborn, E. P. F. Lee, J. M. Dyke, D. W. K. Mok, D. E. Shallcross and C. J. Percival, *Phys. Chem. Chem. Phys.*, 2012, **14**, 10391.
- 45 O. Welz, A. J. Eskola, L. Sheps, B. Rotavera, J. D. Savee, A. M. Scheer, D. L. Osborn, D. Lowe, A. Murray Booth, P. Xiao, M. Anwar H. Kahn, C. J. Percival, D. E. Shallcross, and C. A. Taatjes, *Angew. Chem. Int. Ed.*, 2014, **18**, 4547.
- 46 T. Berndt, J. Voigtländer, F. Stratmann, H. Junninen, R. L. Mauldin III, M. Sipilä, M. Kulmala and H. Herrmann, *Phys. Chem. Chem. Phys.*, 2014, DOI: 10.1039/C4CP02345E
- 47 A. B. Ryzhkov and P. A. Ariya, *Phys. Chem. Chem. Phys.*, 2004, **6**, 5042.
- 48 Y. Scribano, N. Goldman, R. J. Saykally, and C. Leforestier, *J. Phys. Chem. A*, 2006, **110**, 5411.
- 49 L. Sheps, A. M. Scully, and K. Au, *Phys. Chem. Chem. Phys.*, 2014, DOI: 10.1039/c4cp04408h.
- 50 J. M. Anglada, J. Gonzalez, M. Torrent-Sucarrat, *Phys. Chem. Chem. Phys.*, 2011, **13**, 13034.
- 51 W. Adam, R. Curci and J. O. Edwards, *Acc. Chem. Res.*, 1989, **22**, 205.
- 52 R. W. Murray, *Chem. Rev.*, 1989, **89**, 1187.
- 53 R. Curci, A. Dinoi and M. F. Rubino, *Pure & Appl. Chem.*, 1995, **67**, 811.
- 54 D. Heard, *Nature*, 2012, **488**, 164.
- 55 J. Prousek, *Chemické Listy*, 2009, **103**, 271.
- 56 C. A. Taatjes, D. E. Shallcross and C. J. Percival, *Phys. Chem. Chem. Phys.*, 2013, DOI:10.1039/C3CP52842A.